Solid State Communications 389 (2024) 115522

Contents lists available at ScienceDirect

Solid State Communications

journal homepage: www.elsevier.com/locate/ssc

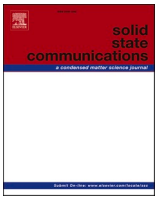

Thermal, optoelectronic and thermoelectric properties of inorganic double perovskites semiconductors Cs_2(Sn, Pt, Te)I_6 for application as intermediate-band solar cells

K. Bouferrache [a], M.A. Ghebouli [b,c], Y. Slimani [d], B. Ghebouli [e], M. Fatmi [b,*], T. Chihi [b], A. Djemli [a,f], Aref Omri [g], Munirah D. Albaqami [h], Saikh Mohammad [h], M. Habila [h], A. Benali [i]

[a] Department of Physics, Faculty of Sciences, University of Mohamed Boudiaf, M'sila, 28000, Algeria
[b] Research Unit on Emerging Materials (RUEM), University Ferhat Abbas of Setif 1, Setif, 19000, Algeria
[c] Department of Chemistry, Faculty of Sciences, University of Mohamed Boudiaf, M'sila, 28000, Algeria
[d] Laboratory of Intelligent System (LSI), Faculty of Technology, University Ferhat Abbas of Setif 1, Setif, 19000, Algeria
[e] Laboratory for the Study of Surfaces and Interfaces of Solid Materials (LESIMS), University Ferhat Abbas of Setif 1, Setif, 19000, Algeria
[f] Faculty of Physics, University of Sciences & Technology Houari Boumediene (U.S.T.H.B), El Alia, BP 32, Bab Ezzouar, 16111, Algiers, Algeria
[g] Faculty of Science and Technology, University of Kairouan, Campus Agricultural City, Sidi Bouzid, 9100, Tunisia
[h] Department of Chemistry, College of Science, King Saud University, P.O. Box 2455, Riyadh, 11451, Saudi Arabia
[i] I3N and Physics Department, University of Aveiro, 3810-193, Aveiro, Portugal

ARTICLE INFO

Communicated by Francois Peeters

Keywords:
Double perovskites semiconductors
Photon energy
Cs_2PtI_6
Cs_2SnI_6
Cs_2TeI_6
Solar cells

ABSTRACT

First-principle calculations using the Wien2k code and the GGA-mBJ exchange potential were used in the study of the thermodynamic, dynamic, chemical and elastic stability, as well as the electronic, optical and thermoelectric properties of Cs_2(Sn, Pt, Te)I_6. The presence of an intermediate band in Cs_2(Sn, Pt, Te)I_6 semiconductors confirmed by absorption peaks appeared at photon energy corresponding to the band gap enhances the efficiency of solar cells. The ideal band gap, high dielectric constants and optimal absorption make the double perovskites under study perform well in solar cells. The calculated minimum formation energy, Helmholtz free energy and phonon modes through the first Brillouin zone for the investigated Cs_2(Sn, Pt, Te)I_6 family confirm their thermal, thermodynamic and dynamic stability. The acoustic phonon contribution modes come from the Cs-6s and I-5p electrons, while the Pt-6s, Sn-5p, Te-5p and I-5p electrons participate in the optical phonon modes. The narrowness of the upper valence band and the band gap in the visible region for Cs_2PtI_6 advantage this double perovskite in energy harvesting. The geometric Goldschmidt tolerance factor value between 0.8 and 1.0 and octahedral factor 0.41 indicate that Cs_2SnI_6 double perovskite is more stable.

1. Introduction

The thermodynamic, dynamic, chemical and elastic stability of double perovskites Cs_2(Sn, Pt, Te)I_6 attract considerable attention from researchers. Materials having intermediate band are identified by fractionation from the band gap to sub-band gaps. The electrons transit from the valence band to the intermediate band then reach the conduction band by absorption of photons. The intermediate band present at the band gap of a material improves the efficiency of solar cells. The improvement in power conversion efficiency (PCE) of materials having intermediate band is attributed to the photovoltaic characteristics of absorber perovskites such as tunable band gap, excellent optical absorption and high stability. Then the design of new intermediate band materials requires high optical absorption, photovoltaic solar energy [1] and achieve high solar conversion efficiencies [2]. The study of the band structure and density of state indicates that Cs_2SnI_6 contains an intermediate band and the additional absorption peaks present confirm it [3]. An electronic structure calculation carried out by Vienna Ab initio simulation package (VASP) using the HSE0677 hybrid functional and includes explicit spin-orbit coupling treatment indicates a direct band gap of Cs_2SnI_6 and Cs_2TeI_6 smaller than the optical band gap [4]. Rb_2PtBr_6 and Rb_2PtI_6 have an optimal band gap in the range 0.9–1.6 eV, the high static dielectric constant indicates a good absorption in visible-light for single junction photovoltaic applications [5]. The

* Corresponding author.
E-mail address: fatmimessaoud@yahoo.fr (M. Fatmi).

https://doi.org/10.1016/j.ssc.2024.115522
Received 10 March 2024; Received in revised form 5 April 2024; Accepted 15 April 2024
Available online 18 April 2024

Table 1
Lattice constant (a_0), bulk modulus (B), pressure derivative of bulk modulus B', minimum energy (E_0) and formation energy ($E_{fomation}$).

	a_0 (Å)	B (GPa)	B'	E_0 (Ry)	$E_{fomation}$ (eV)
Cs_2SnI_6	12.064 12.00 [18] 11.65 exp. [20]	16.37	4.99	−128948.73	−1.88
Cs_2PtI_6	11.744 11.74 [18] 11.37 exp. [19]	24.69	4.30	−153483.71	−1.32
Cs_2TeI_6	12.074 12.06 [18] 11.70 exp. [20]	16.89	4.39	−130184.22	−1.72

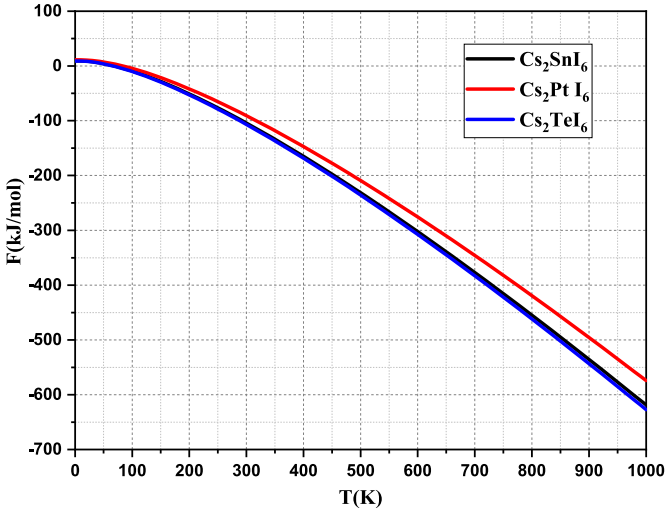

Fig. 1. Helmholtz free energy in the harmonic approximation as function of temperature for Cs_2SnI_6, Cs_2PtI_6 and Cs_2TeI_6.

highest value of the static refractive index of Cs_2PtI_6 indicates a good absorption of the material to the incident spectrum [6]. Perovskite materials are used in solar energy harvesting because of their suitable absorption and band gap [7,8]. Achieving a maximum figure of merit (ZT) requires a high Seebeck coefficient and lower thermal conductivity [9–11]. A high Seebeck coefficient, adequate ZT values make $Cs_2(Se, Sn, Te, Ti)I_6$ attractive for thermoelectric applications [12]. Halide double perovskites have been examined as potential for optoelectronic applications [13]. In this work, we employ the Wien2k computational code within a GGA and mBJ-GGA as exchange potential to investigate the thermodynamic, dynamic, chemical and elastic stability, the electronic, optical and thermoelectric properties of Cs_2(Sn, Pt, Te)I_6. Our studied double perovskites Cs_2SnI_6, Cs_2PtI_6 and Cs_2TeI_6 are suitable thermoelectric materials because of their high figure of merit $(ZT = 1)$, Seebeck $(S = 3000\mu V/K)$ and lower thermal conductivity for P-type carriers. The forbidden band of Cs_2SnI_6, Cs_2TeI_6 and Cs_2PtI_6 localized between 1 and 1.8 eV is suitable for single junction perovskite solar cells. The large static dielectric constant points to the ferroelectric behaviour of these materials. The first imaginary peak of Cs_2SnI_6, Cs_2TeI_6 and Cs_2PtI_6 located at 2 eV, 2.5 eV and 2 eV correspond to the direct (Γ-Γ) and indirect (W-L) and (Γ-X) optical transition from valence band to intermediate band 0.95 eV, 1.829 eV and 1.176 eV. An energy harvesting device was created in order to evaluate its potential as a piezoelectric autonomous power supply [14].

2. Computational details

All physical properties were studied using the computer code Wien2k [15]. The generalized gradient approximation (PBE-GGA) [16] of Perdew, Burke and Ernzerhof was used in the lattice constants optimizing process. The electronic, optical and thermoelectric characterizations were expected by the modified Becke-Johnson exchange potential [17]. We report the product of the smallest muffin-tin sphere radius (R_{MT}) and the largest plane wave vector (K_{max}) of 9. R_{MT} of Cs, Sn, Pt, Te and I takes 2.5 and k-points of Cs_2 (Sn, Pt, Te)I_6 using GGA approaches is 1000 to achieve perfect convergence of energy. Calculation of optical and thermoelectric properties requires k-meshes = 10,000, while 5000 for elastic constants. The maximum radial expansion $I_{max} = 10$ is the value used for performing this self-consist calculations. The E^{cut}_{off} between the valence states and the nucleus was - 8 Ry, while 10^{-3} e is chosen as the convergence charge. Valence electrons form chemical bonds, while those in the nucleus ensures the chemical reactivity of an atom. The electronic configuration of these elements is Cs: [Xe] $6s^1$, Sn: [Kr] $4d^{10}5s^25p^2$, Pt: [Xe] $4f^{14}5d^96s^1$, Te: [Kr] $4d^{10}5s^25p^4$ and I: [Kr] $4d^{10}$ $5s^25p^5$. We note that R_{MT} effect on electronic characteristics is not decisive with respect to the GGA-mBJ exchange potential. GGA-mBJ corrects the formation energy, transition energy level, lattice constant, electrostatic potential, valence band maximum and total energy. The formation energy of compound is that which disperses it into isolated atoms when all the bonds are broken.

3. Results and discussions

3.1. Thermal, thermodynamic, dynamic and mechanical stability

$Cs_2(Sn, Pt, Te)I_6$ double perovskites crystallize in a face centered cubic structure with space group $Fm\bar{3}m(\#225)$, where Cs atoms are in the spaces between the octahedrons 8c (0.25, 0.25, 0.25), (Sn, Pt, Te) atoms occupy 4a (0, 0, 0), and the I atoms are at positions 24e (x, 0, 0), where the value of x is 0.2296. Calculation of Goldschmidt tolerance factor (t) and octahedral factor (μ) is necessary for knowledge of structural stability and predicting the application domain with high performance. Experimental research and simulation limit the number of compounds of interest for optoelectronics by evaluating the geometric Goldschmidt tolerance factor $t = \frac{(r_{Cs}+r_{(Sn,Pt,Te)})}{\sqrt{2}(r_{(Sn,Pt,Te}+r_I)}$ [18] and octahedral factor $u = \frac{r_{(Sn,Pt,Te)}}{r_I}$ [19], where r_{Cs}, $r_{(Sc,Pt,Te)}$, r_I are the ionic radii for ions Cs, (Sn, Pt, Te) and I sites. An ideal double perovskite shows a tolerance factor t = 1. When the ratio of ionic radii deviates from unity, geometric deformation and crystal distortions appear [20]. The values for Cs_2SnI_6, Cs_2PtI_6 and Cs_2TeI_6 of Goldschmidt tolerance factor (octahedral factor) are 0.85, 0.91 and 0.62 (0.53, 0.36 and 1) with their theoretical ones 0.99, 1.02 and 0.91 (0.31, 0.28 and 0.44) [18] indicate that Cs_2SnI_6 double perovskite is more stable because it has t value between 0.8 and 1.0 and a u value greater than 0.41. The optimization of the compounds under study to obtain a minimum fundamental energy, the lattice constant, the bulk modulus and its derivative with respect to the pressure, as well as the formation energy are listed in Table 1. The lattice constant of our perovskites agrees with their available experimental data [21,22] and theoretical ones calculated using the GGA-PBE functional [23]. The negativity of $Cs_2(Sn, Pt, Te)I_6$ minimum energy and formation energy translates their chemical and thermal stability calculated from the following expression:

$$E^{Cs_2(Sn,Pt,Te)I_6}_{form} = E^{Cs_2(Sn,Pt,Te)I_6}_{tot} - \frac{E^{Cs}_{tot}}{2} - E^{(Sn,Pt,Te)}_{tot} - \frac{E^{I}_{tot}}{6} \quad (1)$$

The total and formation energies of these perovskites traduce their chemical and thermal stability. Chemical stability is more pronounced in Cs_2PtI_6, while Cs_2SnI_6 is more thermally stable. Fig. 1 illustrates the evolution of the Helmholtz free energy as a function of temperature for Cs_2(Sn, Pt, Te)I_6 in the harmonic approximation. These perovskites are reported to be thermodynamically stable because of their negative Helmholtz free energy, which decreases with increasing temperature. This stability is more pronounced in $Cs_2(Te, Sn)I_6$.

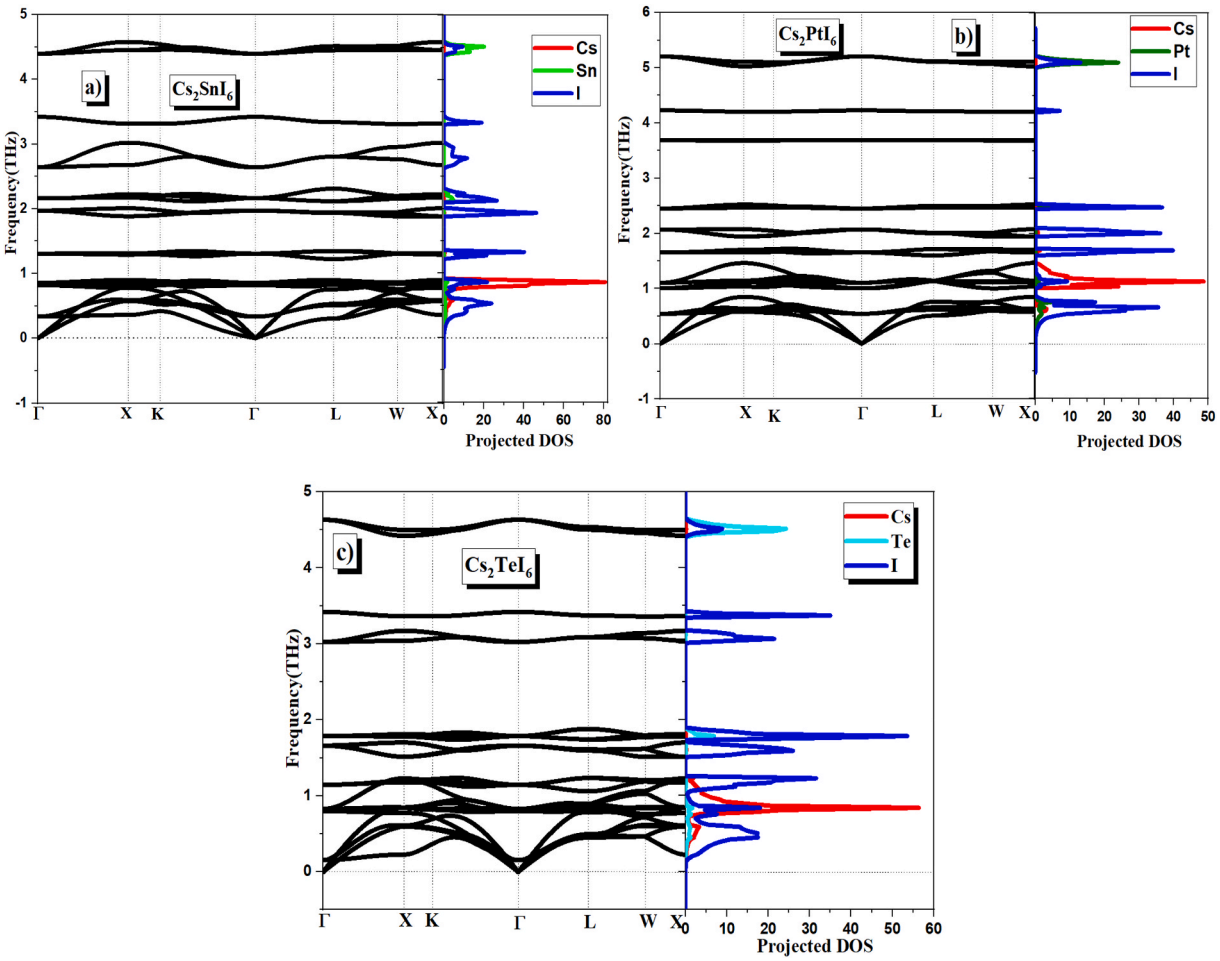

Fig. 2. Phonon dispersions curves and projected density of states for Cs_2SnI_6 (a), Cs_2PtI_6 (b) and Cs_2TeI_6 (c) computed by Phonopy with GGA approaches.

Table 2
Elastic constants, shear modulus, bulk modulus, anisotropy factor, Young's modulus, Poisson's ratio and B_H/G_H ratio for $Cs_2(Sn, Pt, Te)I_6$.

$$0 \prec C_{11}, 0 \prec C_{44}, 0 \prec C_{11} - C_{12}, 0 \prec C_{11} + 2C_{12}, C_{12} \prec B \prec C_{11} \quad (2)$$

	Cs_2SnI_6	Cs_2PtI_6	Cs_2TeI_6
C_{11} (GPa)	30.52	36.05	38.51
	17.7 [21]	9.58 [20]	20.3
C_{12} (GPa)	9.19	7.20	6.059
	11.8 [21]	4.51 [20]	10.55
C_{44} (GPa)	8.3158	8.31	6.5869
	8.99 [21]	3.93 [20]	8.70
G_v (GPa)	9.25	10.75	10.44
G_R (GPa)	9.11	10.00	8.63
G_H (GPa)	9.18	10.38	9.54
B_H (GPa)	16.30	16.81	16.87
A	0.77	0.57	0.40
E_V (GPa)	23.34	26.59	25.96
E_R (GPa)	23.05	25.05	22.13
E_H (GPa)	23.20	25.82	24.08
σ_V	0.26	0.23	0.24
σ_H	0.26	0.24	0.26
σ_R	0.26	0.25	0.28
B_H/G_H	1.77	1.61	1.76
Transverse elastic wave velocity (m/s)	1455.93	2032.57	1479.71
Longitudinal elastic wave velocity (m/s)	2566.95	3368.38	2606.26
Average wave velocity (m/s)	1618.82	2247.26	1645.12
Debye Temperature (K)	131.89	187.83	133.93
Melting Temperature (K)	733.40	1186.96	780.60

We present in Fig. 2 the phonon dispersions curves and projected density of states for Cs_2SnI_6, Cs_2PtI_6 and Cs_2TeI_6 computed by Phonopy with GGA approaches. It is reported that no negative frequency phonon modes through the first Brillouin zone are observed, confirming their dynamic stability. We note also that the acoustic phonon contribution modes come from the Cs-6s and I-5p electrons, while the Pt-6s, Sn-5p, Te-5p and I-5p electrons participate in the optical phonon modes for all perovskites. The high anharmonic lattice dynamic of $Cs_2(Sn, Pt, Te)I_6$ reduces their thermal conductivity, giving them an advantage of use in the thermoelectric field. The mechanical stability and related characteristics of the double perovskites with cubic symmetry Cs_2(Sn, Pt, Te)I_6 are determined using the elastic constants C_{11}, C_{12}, C_{44} and the bulk modulus B using finite strain theory as shown in Table 2. We note that all elastic moduli verify the stability criteria, hence their mechanical stability.

The fairly large inter reticular distances of these double perovskites is qualitatively explained by their lower binding ionic forces, their weaker elastic constants and lower hardness, which make them as soft and tolerant to damage [24]. The bulk and shear modulus, universal anisotropy factor, Young's modulus, Poisson's ratio and Pugh coefficient of isotropic polycrystalline materials are reported in Table 2 using the Voigt-Reuss-Hill approximation. The low values of bulk modulus, shear modulus and Young's modulus of these double perovskites confirm their lower hardness and rigidity. The Poisson's ratio is in the range 0.16–0.30 reflects the ionic-covalent bonds. The three-dimensional representation of Young's modulus and Poisson's ratio is illustrated in Fig. 3. These two parameters in the double perovskites under study are reported to be anisotropic in all three directions. The Pugh's criterion (B_H/G_H) and

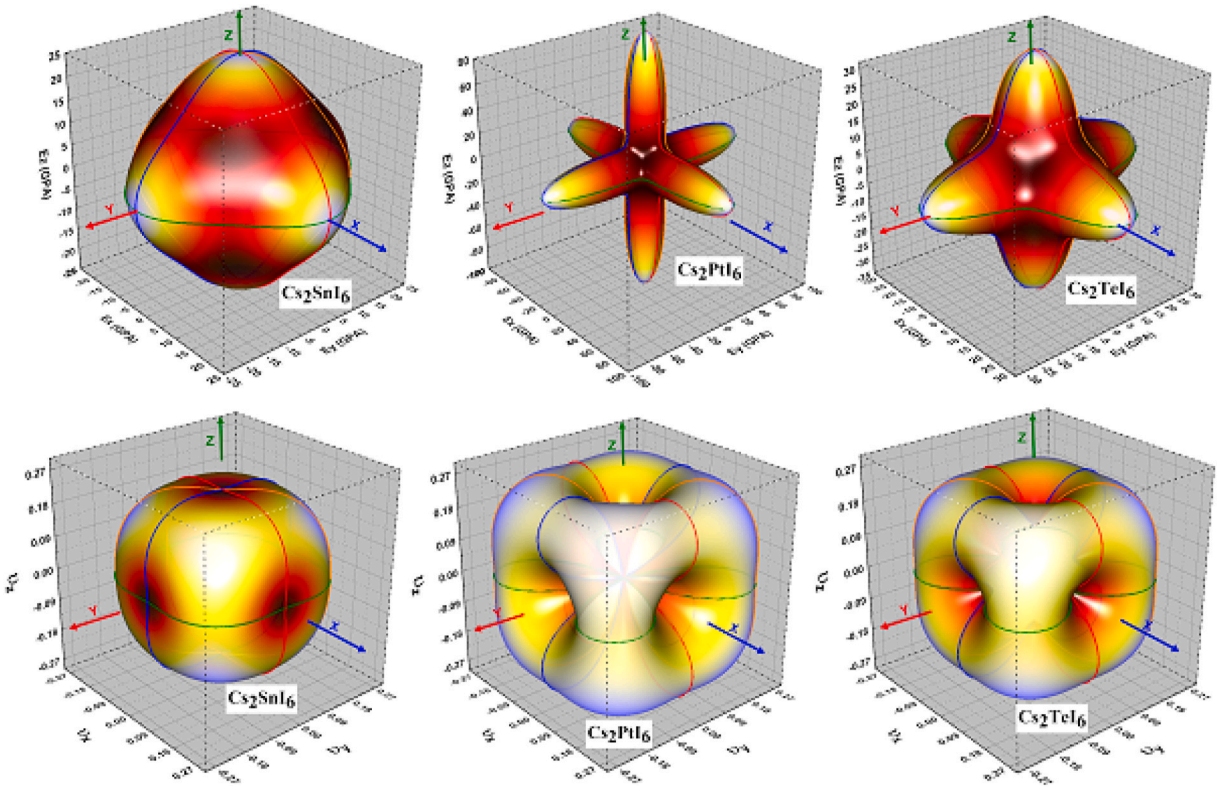

Fig. 3. 3D surface of Young's modulus and Poisson's ratio for Cs_2SnI_6, Cs_2PtI_6, Cs_2TeI_6.

Table 3
The band gap of $Cs_2(Sn, Pt, Te)I_6$ calculated using GGA and mBJ-GGA.

	E_g (eV) GGA	E_g (eV) mBJ-GGA	E_g exp. (eV)	E_g theo. (eV)
Cs_2SnI_6	0.274	0.95	1.25 [27]	0.84 [23]
Cs_2PtI_6	0.621	1.176	1.37 [25]	1.07 [23]
Cs_2TeI_6	1.391	1.829	1.50 [26]	1.70 [23]

universal anisotropy factor (A) indicate that Cs_2SnI_6 and Cs_2TeI_6 are ductile, while Cs_2PtI_6 is brittle and all compounds are anisotropic. Table 2 lists the transverse, longitudinal and average elastic wave velocities, the Debye temperature, which is a characteristic of the behavior of heat capacity and hardness and the melting point at which the substance changes state from solid to liquid.

3.2. Optoelectronic characteristics

The band gap underestimation by the semi-local functional GGA of $Cs_2(Sn, Pt, Te)I_6$ is related to the binding energy of half-core Sn-5p, Pt-6s, Te-5p levels, therefore we use the mBJ-GGA functional, where the precision is better. The band gap of $Cs_2(Sn, Pt, Te)I_6$ calculated using GGA and mBJ-GGA functionals are reported in Table 3. The energy gap of our perovskites is in good agreement with those calculated experimentally [25–27] and other theoretical one using other functionals such as PBE+SOC, HSE06, HSE06+SOC and G_0W_0 [23]. Electronic band structure and density of states using mBJ-GGA for Cs_2SnI_6, Cs_2TeI_6 and Cs_2PtI_6 are reported in Fig. 4. We conclude from the band structure that the band gap is indirect nature W-L and Γ-L for Cs_2TeI_6 and Cs_2PtI_6, while it is direct Γ-Γ in Cs_2SnI_6. It is reported that band gap of Cs_2SnI_6 and Cs_2TeI_6 are direct Γ-Γ and indirect X-L [28]. The band gap of Cs_2PtI_6 and Cs_2SnI_6 are in good concordance with other reported calculation 1.35 eV and 1.23 eV [23]. We note that the upper valence band is narrower in the Cs_2PtI_6 perovskite. The forbidden band in visible region is an advantage for the energy harvesting property. The PDOS shows that the valence band near the Fermi level consists of the occupied I-5p orbital, while the empty orbital in the first conduction band is Cs-6s, and therefore the electronic transition will take place between these two orbitals in all perovskites.

I atoms draw so much charge because of their high electronegativity compared to Sn, Pt, Te atoms. The significant charge between (Sn, Pt, Te)-I bonds due to the low difference in electronegativity and the hybridization between I-5p and (Sn-5p, Pt-6s, Te-5p) levels translate their covalent bonding. The upper valence band of these perovskites are dominated by I-p orbitals, while conduction band minimum is contributed by I-p orbitals along with Pt-d, Te-p and Sn-s orbitals in Cs_2PtI_6, Cs_2TeI_6 and Cs_2SnI_6. Maintaining high power conversion efficiency requires a band gap in the range 1 eV–1.8 eV and a polarization orientation along the a-axis for cubic structure [29–31], then Cs_2PtI_6, Cs_2TeI_6 and Cs_2SnI_6 are suitable for single junction perovskite solar cells. Halide perovskites are responsible for the high efficiency of solar cells [32].

Fig. 5 shows the imaginary (a) and real (b) parts of the dielectric function, the refractive index (c), the extinction coefficient (d), the energy loss (e), the absorption coefficient (f), The real (g) and imaginary (h) parts optical conductivity and the reflectivity (i) as a function of photon energy for Cs_2SnI_6, Cs_2TeI_6 and Cs_2PtI_6 double perovskites using mBJ-GGA. Knowledge of the optical values of a material makes it possible to specify its practical field of application. The dielectric function of a material is expressed in terms of their real and imaginary parts by:

$$\varepsilon = \varepsilon_r + \varepsilon_i \tag{3}$$

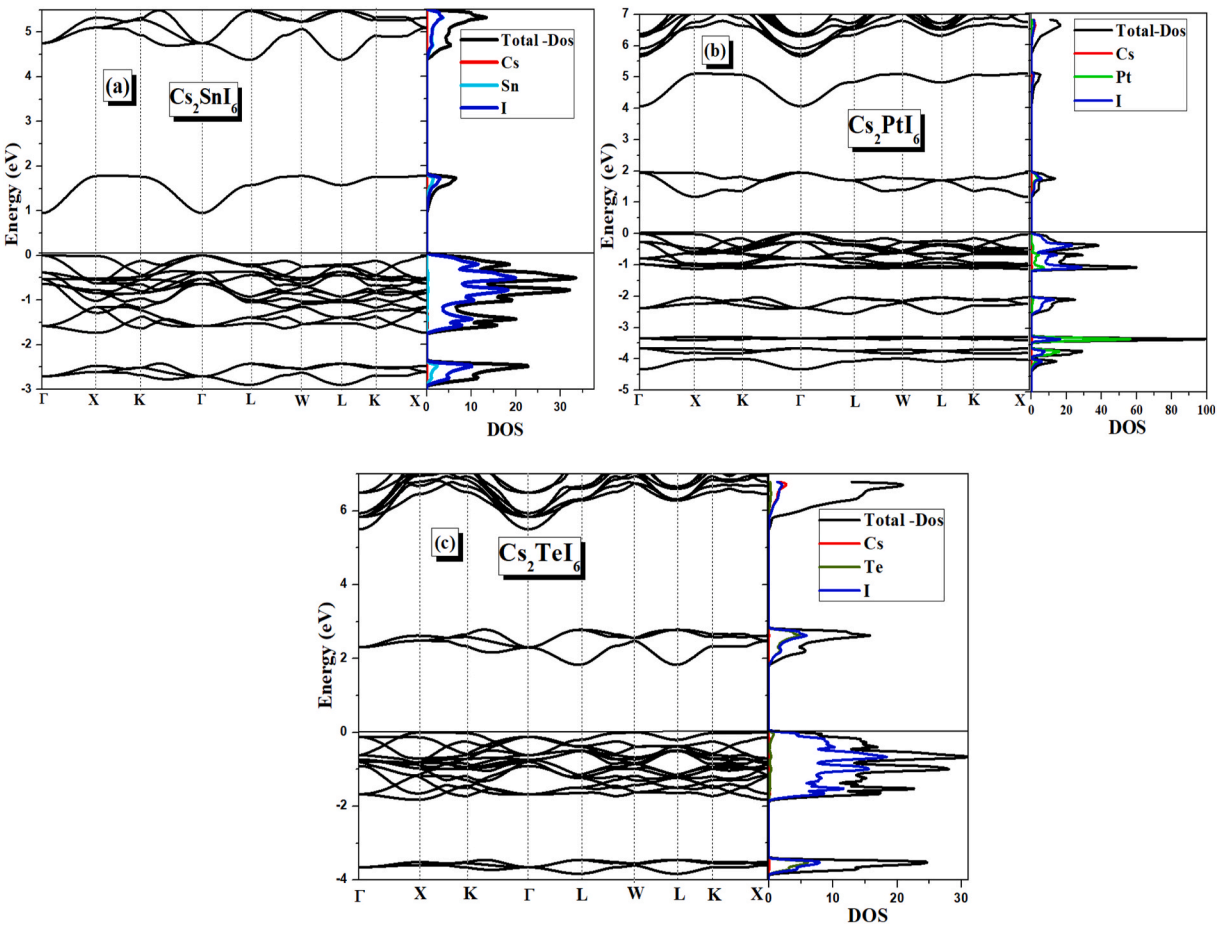

Fig. 4. Electronic band structure and density of states for Cs_2SnI_6 (a), Cs_2PtI_6 (b) and Cs_2TeI_6 (c) using mBJ-GGA.

The real part specifies the degree of polarization, indicates capacitive or inductive optical response of a material and it is more important in the visible region. While, the imaginary part which is due to dielectric losses, tells us about the resistivity of a material. It is always positive and represents the energy absorbed by such a material. The static dielectric constant $\varepsilon_r(0)$ calculated using TB-mBJ for Cs_2SnI_6, Cs_2TeI_6 and Cs_2PtI_6 is 14.49, 12.57 and 26.42. It reaches a maximum value of 20, 22 and 50. The large static dielectric constant arises from the lattice contribution and points to the ferroelectric behavior of the material. The real dielectric constant of these double perovskites is smaller at high frequency, this leads to their weaker response to external fields. The imaginary part of the dielectric constant for Cs_2SnI_6, Cs_2PtI_6 and Cs_2TeI_6 starts at 0.9 eV, 1.1 eV and 1.8 eV, which corresponds to the band gap. The first imaginary peak of Cs_2SnI_6, Cs_2TeI_6 and Cs_2PtI_6 located at 2 eV, 2.5 eV and 2 eV correspond to the direct (Γ-Γ) and indirect (W-L) and (Γ-X) optical transition from valence band to intermediate band 0.95 eV, 1.829 eV and 1.176 eV. The refractive index of a semiconductor material is linked to the speed of propagation of light in a medium, and it is correlated to the optical band gap. The static refractive index of Cs_2SnI_6, Cs_2PtI_6 and Cs_2TeI_6 is 3.80, 5.14 and 3.54. The static refractive index reaches a maximum value and then rapidly decreases in a linear manner. We note that optical properties such as static refractive index and dielectric constant are proportional to the band gap. The extinction coefficient quantifies the proportion of light lost due to scattering and absorption per unit distance from a medium. It follows the same variation as that of the imaginary part, and it is greater at low energy, and it decreases in the sequence $Cs_2TeI_6 \rightarrow Cs_2PtI_6 \rightarrow Cs_2SnI_6$. The absorption coefficient depends on the energy of the incident photon, according to the condition of the transition, where the transition occurs only when the energy of the photon is equal or greater than the value of the band gap. The thresholds are closer to the calculated band gap and are attributed to the inter-band electronic transitions. Absorption significantly influences the property of materials for solar cells. The absorption coefficient shows that absorption begins from the energies which correspond to the band gap of a material. Absorption in the visible range is less significant than that in the ultraviolet light. The significant absorption in the ultraviolet region and the adequate band gap allow us the use of these double perovskites in the photovoltaic field. The absorption peak was observed at photon energy 2 eV, 2 eV, 2.5 eV for Cs_2SnI_6, Cs_2PtI_6 and Cs_2TeI_6. Cs_2SnI_6 and Cs_2PtI_6 have fewer losses of 10–30 % in the visible and ultraviolet. The real part of the optical conductivity shows a similar shape as that of the imaginary part of the dielectric constant and increases with increasing photon energy. Conductivity begins with the start of absorption. The imaginary part of optical conductivity can take negative values. Negative optical conductivity is linked to a possible inter-bond transitions and transport relaxation time. The static optical reflectivity is 33 %, 31 % and 46 % for Cs_2SnI_6, Cs_2TeI_6 and Cs_2PtI_6. The reflectivity increases in the visible region, then it stagnates in the ultraviolet around 30 %. High optical absorption in the ultraviolet light provides information on solar energy

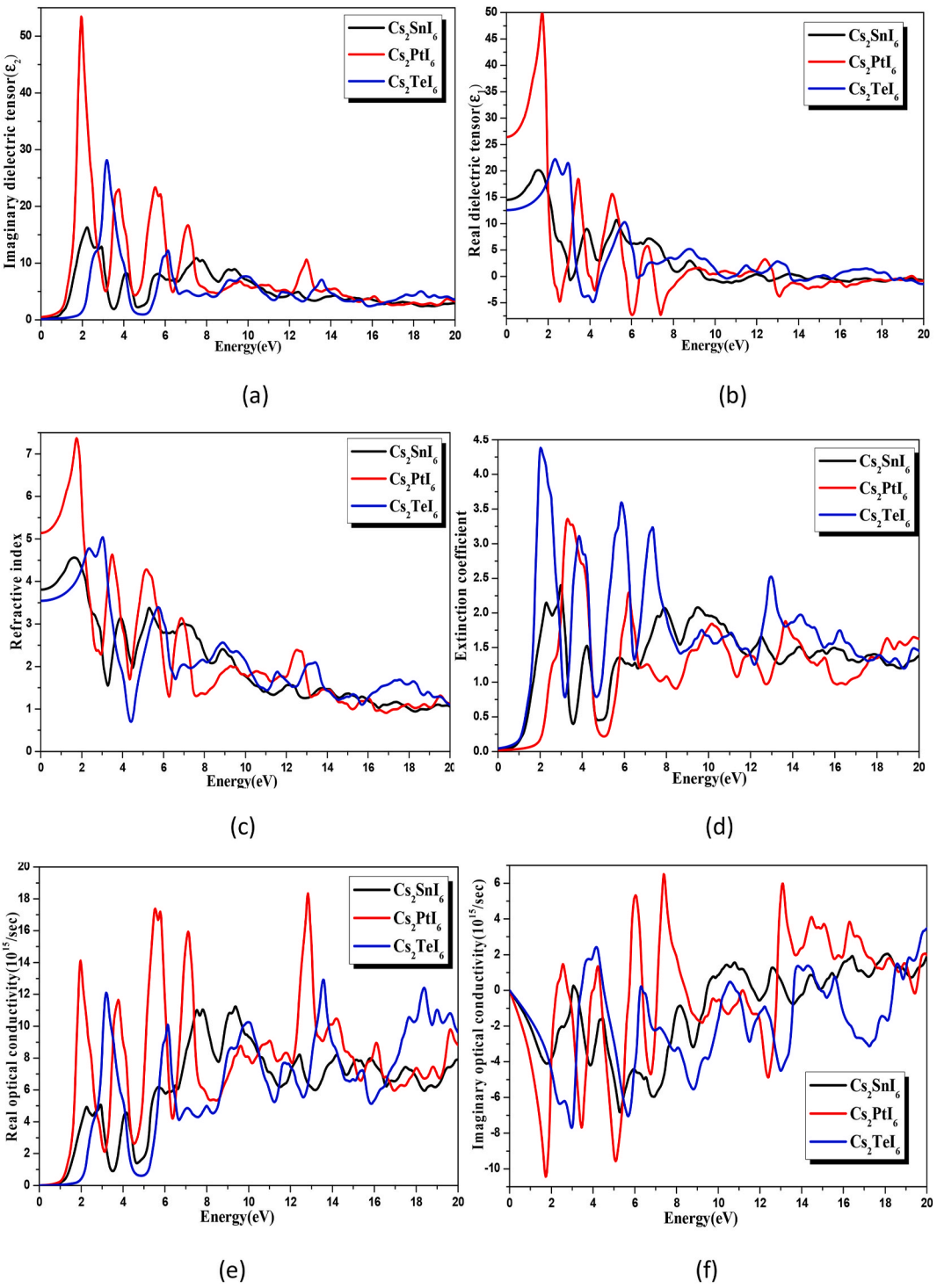

Fig. 5. The real (a) and imaginary (b) parts of the dielectric function, the refractive index (c), the extinction coefficient (d), the energy loss (e), the absorption coefficient (f), The real and imaginary (g) parts optical conductivity (h) the reflectivity (i), as a function of photon energy for Cs_2(Sn, Pt, Te)I_6 perovskites using mBJ-GGA.

conversion and efficiency for materials application in the photovoltaic field and makes them favorable for optical devices working in this range.

3.3. Thermoelectric properties

The study of the thermoelectric properties of these double perovskites was made using the BoltzTrap Code 58 [33]. Figs. 6 and 7 show the effect of charge carrier concentration (N) and temperature (T) on the Seebeck coefficient, electronic thermal conductivity, the thermal conductivity, the figure of merit ZT and power factor for Cs_2(Sn, Pt, Te)I_6. The Seebeck coefficient is a measure of the ratio between induced voltage and temperature variation accros the material. The top of the valence band is reported to coincide with N = 0. We can see that for N negative, the Seebeck is positive for Cs_2(Sn, Pt, Te)I_6 at T = 300 K,

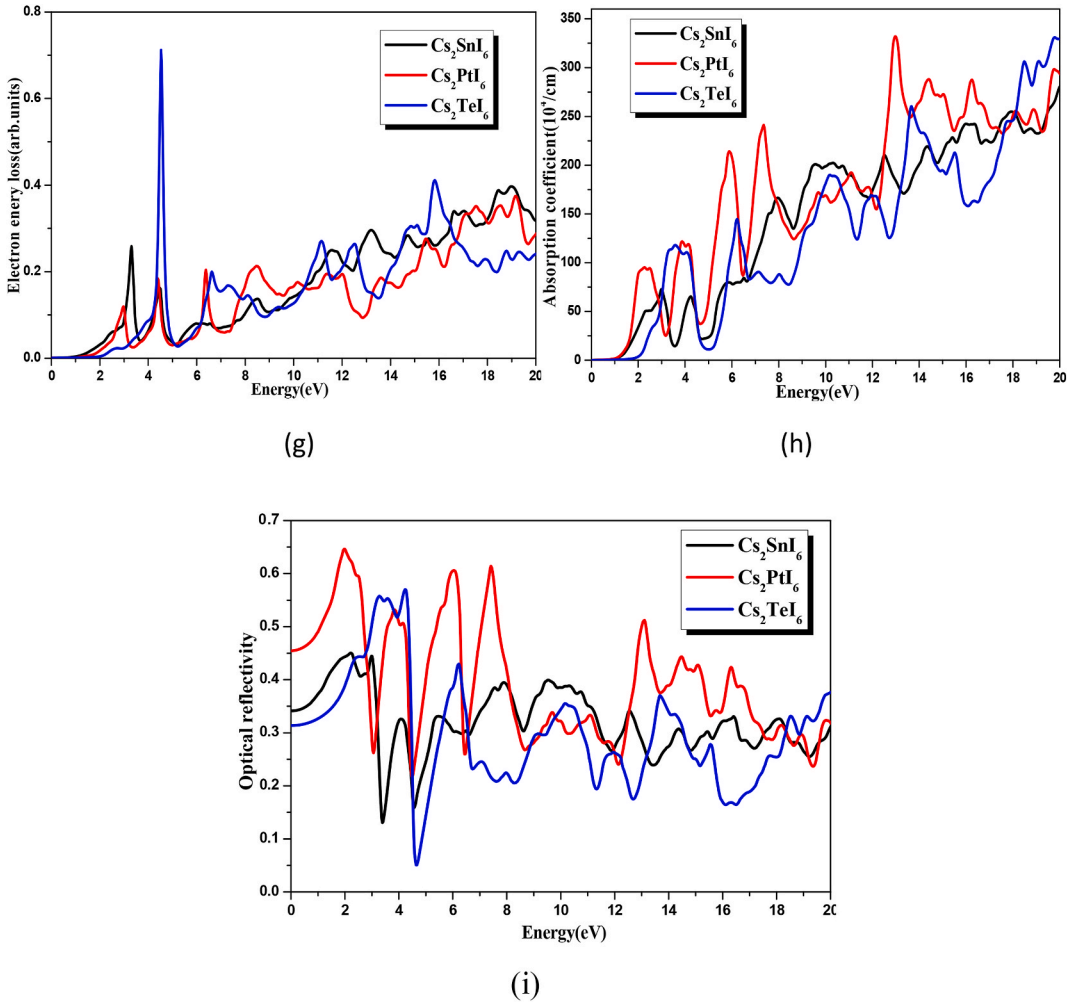

Fig. 5. (*continued*).

indicating that these double perovskites are p-type semiconductors. The maximum values of Seebeck for Cs_2SnI_6, Cs_2PtI_6 and Cs_2TeI_6 are obtained at N = 2 e/uc, 4 e/uc and 7 e/uc. We can see that the value of Seebeck decreases with an increase in temperature for all the considered Cs_2(Sn, Pt, Te)I_6 double perovskites. The S increases following sequences $Cs_2TeI_6 \rightarrow Cs_2PtI_6 \rightarrow Cs_2SnI_6$ in the temperature interval 100 K–600 K. The Seebeck value at 300 K for Cs_2TeI_6, Cs_2PtI_6 and Cs_2SnI_6 is 200 μV/K, 220 μV/K and 230 μV/K. Efficient thermoelectric material exhibits low electronic thermal conductivity, which depends on network dynamics. Network dynamics influence electronic thermal conductivity and optical emission. This results in significant phonon-phonon scattering, which leads to low electronic thermal conductivities and better thermoelectric performance. Low electronic thermal conductivity is achieved in p-type semiconductors Cs_2(Sn, Pt, Te)I_6. The efficiency of the materials under study in the conversion of heat into electrical energy is present, since p-type charge carriers give almost a factor of merite 100 %, and at 100 K. it is estimated at 83 %, 80.5 % and 78 % for Cs_2SnI_6, Cs_2TeI_6 and Cs_2PtI_6. These data make these double perovskites promising for thermoelectric applications. The substitution of Sn by Pt and Te affects little the electronic thermal conductivity at low temperature, while replacing Sn by Pt (Sn by Te) increases (decreases) at high temperature. The electronic thermal conductivity for Cs_2SnI_6, Cs_2TeI_6 and Cs_2PtI_6 at 300 K is 1.5 W/mK, 0.8 W/mK and 1 W/mK. It is observed in all studied double perovskites that the conductivity is higher in the case where the charge carriers are n-type. Thermal conductivity refers to the intrinsic ability of a given material to conduct or transfer heat. The thermal conductivity increases quadratically with temperature in the sequences $Cs_2TeI_6 \rightarrow Cs_2SnI_6 \rightarrow Cs_2PtI_6$. Analysis of figure of merit reveals highest ZT values (1) for P-type semiconductors. The figure of merit as a function of temperature shows the same trend as that of Seebeck. An almost constant character is observed beyond 500 K. Increasing temperature reduces the band gap of the material and the figure of merit ZT and affects the thermoelectric performance.

4. Conclusion

The ideal band gap obtained for Cs_2(Sn, Pt, Te)I_6 in the optimal range 0.9–1.8 eV using mBJ-GGA indicates that all compounds are potential candidates for single junction solar cells. We explore Cs_2(Sn, Pt, Te)I_6 as potential thermoelectric materials because of their intrinsic p-type conductivity. Efficient and high-performance thermoelectric materials such as Cs_2(Sn, Pt, Te)I_6 exhibit low electronic thermal conductivity due to phonon-phonon scattering and optical emission. The weaker elastic constants explain the large inter reticular distances and lower hardness and binding ionic forces. The analysis of electronic structures proves that the band gap and optical gap in these materials are dictated by the energies of the empty (Sn-5s, Te-5p and Pt-6s) states at the lowest unoccupied band. The efficiency of Cs_2SnI_6, Cs_2TeI_6 and Cs_2PtI_6 in the conversion of heat into electrical energy is due to the p-type charge carriers, which give almost a factor of merite estimated at 83 %, 80.5 % and 78 %. The considerable charge in the (Sn, Pt, Te)-I bonds due to a small difference in electronegativity and the hybridization between these levels reflects their covalent bands.

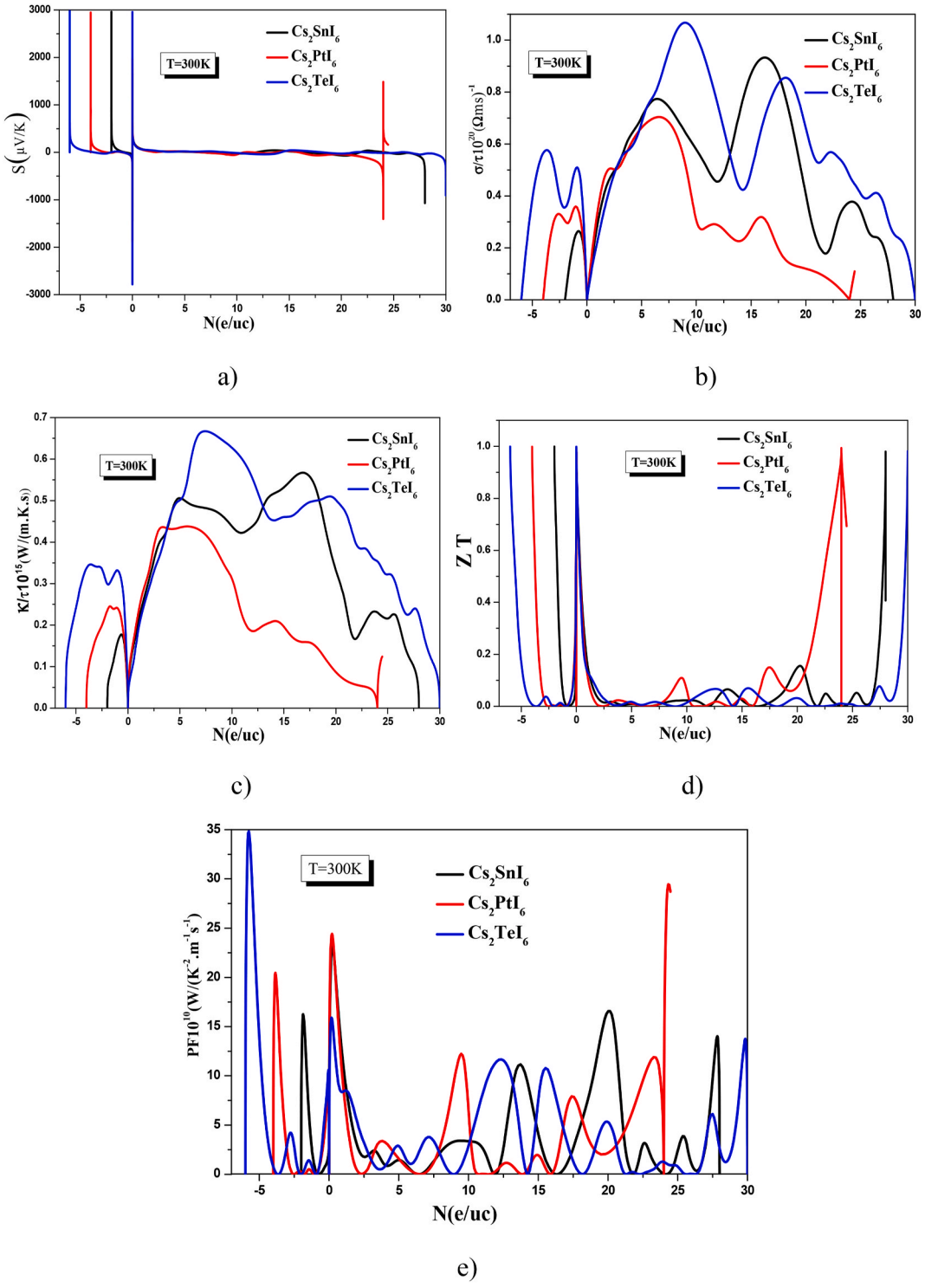

Fig. 6. Charge carriers concentration dependence of, (a) the Seebeck coefficient, (b) electronic thermal conductivity, (c) the thermal conductivity, (d) the figure of merit ZT, (e) power factor at T = 300 K for Cs_2(Sn, Pt, Te)I_6.

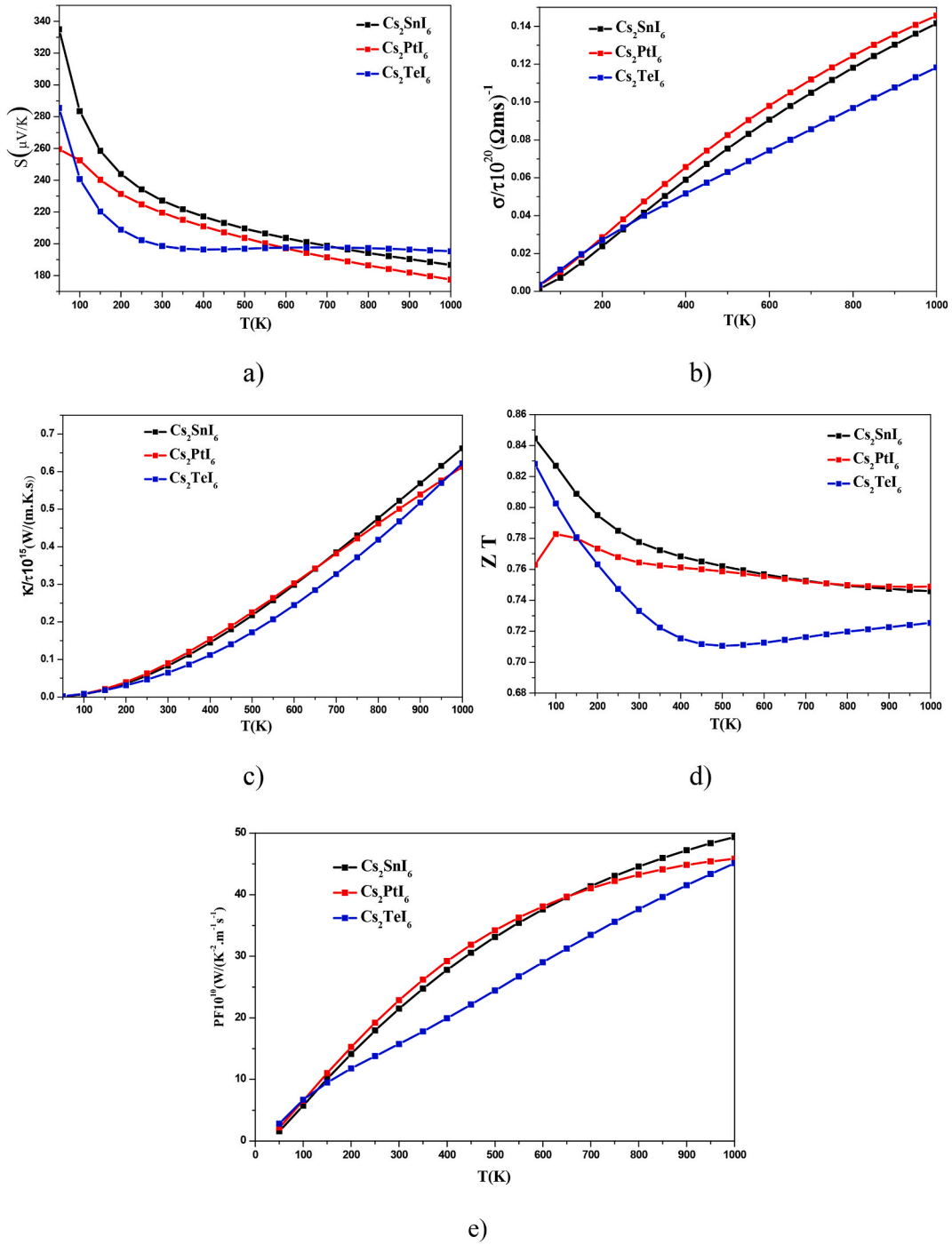

Fig. 7. Temperature dependence of, (a) the Seebeck coefficient, (b)electronic thermal conductivity, (c) the thermal conductivity, (d) the figure of merit ZT, e) power factor for Cs_2(Sn, Pt, Te)I_6 perovskites within mBJ-GGA approximation.

CRediT authorship contribution statement

K. Bouferrache: Investigation. **M.A. Ghebouli:** Resources. **Y. Slimani:** Supervision. **B. Ghebouli:** Software. **M. Fatmi:** Validation. **T. Chihi:** Supervision. **A. Djemli:** Supervision, Software. **Aref Omri:** Methodology. **Munirah D. Albaqami:** Writing - review & editing. **Saikh Mohammad:** Project administration. **M. Habila:** Supervision. **A. Benali:** Investigation, Funding acquisition.

Declaration of competing interest

The authors declared no potential conflicts of interest with respect to the research, authorship, and/or publication of this article.

Data availability

The authors do not have permission to share data.

Acknowledgement

This work was funded by the Researchers Supporting Project Number (RSP2024R267) King Saud University, Riyadh, Saudi Arabia.

References

[1] M. Wolf, Limitations and possibilities for improvement of photovoltaic solar energy converters: Part I: considerations for earth's surface operation, Proc. IRE 48 (1960) 1246–1263.

[2] A. Luque, A. Martí, Increasing the efficiency of ideal solar cells by photon induced transitions at intermediate levels, Phys. Rev. Lett. 78 (1997) 5014.

[3] M. Rasukkannu, D. Velauthapillai, P. Vajeeston, A first-principle study of the electronic, mechanical and optical properties of inorganic perovskite Cs2SnI6 for intermediate-band solar cells, Mater. Lett. 218 (2018) 233–236.

[4] A.E. Maughan, A.M. Ganose, M.M. Bordelon, E.M. Miller, D.O. Scanlon, J. R. Neilson, Defect tolerance to intolerance in the vacancy-ordered double perovskite semiconductors Cs2SnI6 and Cs2TeI6, J. Am. Chem. Soc. 138 (27) (2016) 8453–8464.

[5] M. Faizan, K.C. Bhamu, S.H. Khan, G. Murtaza, Xin He, Computational study of defect variant perovskites A2BX6 for photovoltaic applications, Mater. Sci. (2020).

[6] H. AbdelAziz, M. Taha, W.M.A. El Rouby, M.H. Khedr, L. Saad, Evaluating the performance of Cs2PtI6− xBrx for photovoltaic and photocatalytic applications using first-principles study and SCAPS-1D simulation, Heliyon 8 (10) (2022) e10808.

[7] W. Wang, M.O. Tadé, Z. Shao, Research progress of perovskite materials in photocatalysis-and photovoltaics-related energy conversion and environmental treatment, Chem. Soc. Rev. 44 (15) (2015) 5371–5408.

[8] M. Singh, I. Sinha, Halide perovskite-based photocatalysis systems for solar-driven fuel generation, Sol. Energy 208 (2020) 296–311.

[9] H.J. Goldsmid, Introduction to thermoelectricity, Springer Mater. Sci. 121 (2010).

[10] T. Zhu, Y. Liu, C. Fu, J.P. Heremans, J.G. Snyder, X. Zhao, Compromise and synergy in high-efficiency thermoelectric materials, Adv. Mater. 29 (14) (2017) 1605884.

[11] H. Xie, X. Su, T.P. Bailey, C. Zhang, W. Liu, C. Uher, X. Tang, M.G. Kanatzidis, Anomalously large Seebeck coefficient of CuFeS2 derives from large asymmetry in the energy dependence of carrier relaxation time, Chem. Mater. 32 (6) (2020) 2639–2646.

[12] K. Bouferrache, M.A. Ghebouli, B. Ghebouli, Mohamed A. Habila, T. Chihi, M. Fatmi, A. Djemli, Mika sillanpaa, Results Phys. 56 (2024) 107138.

[13] Yanmeng Chu, Yue Hu, Zewen Xiao, J. Phys. Chem. C 125 (2021) 9688–9694.

[14] Lun Meng-Meng, Luo Jia-Qi, Zhi-Xu Zhang, Jie Li, Li-Yan Xie, Hai Feng Lu, Yi Zhang, Da-Wei Fu, Chem. Eng. J. 475 (2023) 145969, https://doi.org/10.1016/j.cej.2023.145969.

[15] K. Bouferrache, M.A. Ghebouli, Y. Slimani, B. Ghebouli, M. Fatmi, T. Chihi, Norah Algethami, Saif A. Mouhammad, Sultan Alomairy, Elkenany B. Elkenany, Structural stability, opto-electronic, magnetic and thermoelectric properties of half-metallic ferromagnets quaternary Heusler alloys CoFeXAs (X= Mn, Cr and V), Solid State Commun. 377 (2024) 115366–115383.

[16] K. Burke, J.P. Perdew, M. Ernzerhof, Why semilocal functionals work: accuracy of the on-top pair density and importance of system averaging, J. Chem. Phys. 109 (10) (1998) 3760–3771.

[17] A.D. Becke, E.R. Johnson, A simple effective potential for exchange, AIP 124 (22) (2006).

[18] V.M. Goldschmidt, Die gesetze der krystallochemie, Naturwiss 14 (21) (1926) 477–485.

[19] C. Li, K.C.K. Soh, P. Wu, Formability of ABO3 perovskites, J. Alloys Compd. 372 (1–2) (2004) 40–48.

[20] D. Ji, S. Feng, L. Wang, S. Wang, M. Na, H. Zhang, C. Zhang, X. Li, Interface optimization of free-standing CdZnTe films for solar-blind ultraviolet detection: substrate dependence, Vacuum 164 (2019) 186–193.

[21] M. Faizan, K. Bhamu, G. Murtaza, X. He, N. Kulhari, M.M. AL-Anazy, S.H. Khan, Electronic and optical properties of vacancy ordered double perovskites A2BX6 (A= Rb, Cs; B= Sn, Pd, Pt; and X= Cl, Br, I): a first principles study, Sci. Rep. 11 (1) (2021) 1–9.

[22] A.E. Maughan, A.M. Ganose, M.M. Bordelon, E.M. Miller, D.O. Scanlon, J. R. Neilson, Defect tolerance to intolerance in the vacancy-ordered double perovskite semiconductors Cs2SnI6 and Cs2TeI6, J. Am. Chem. Soc. 138 (27) (2016) 8453–8464.

[23] P. Bhumla, M. Jain, S. Sheoran, S. Bhattacharya, Vacancy-ordered double perovskites Cs2BI6 (B= Pt, Pd, Te, Sn): an emerging class of thermoelectric materials, J. Phys. Chem. Lett. 13 (50) (2022) 11655–11662.

[24] Y. Naceur, H. Bourbaba, M.A. Ghebouli, L. Krache, B. Ghebouli, T. Chihi, M. Fatmi, Sultan Alomairy, Ab-initio Study of structural, elastic, electronic and optical properties of hexahalometallate single crystals K2XBr6 (X= Se, Pt), Sci. Rep. 12 (1) (2022) 1–13.

[25] S. Yang, L. Wang, S. Zhao, A. Liu, Y. Zhou, Q. Han, F. Yu, L. Gao, C. Zhang, T. Ma, Novel lead-free material Cs2PtI6 with narrow bandgap and ultra-stability for its photovoltaic application, ACS Appl. Mater. Interfaces 12 (40) (2020) 44700–44709.

[26] I. Vazquez-Fernandez, S. Mariotti, O.S. Hutter, M. Birkett, T.D. Veal, T.D. Hobson, L.J. Phillips, L. Danos, P.K. Nayak, H.J. Snaith, W. Xie, M.P. Sherburne, M. Asta, K. Durose, Vacancy-ordered double perovskite Cs2TeI6 thin films for optoelectronics, Chem. Mater. 32 (15) (2020) 6676–6684.

[27] A.E. Maughan, A.M. Ganose, M.M. Bordelon, E.M. Miller, D.O. Scanlon, J. R. Neilson, Defect tolerance to intolerance in the vacancy-ordered double perovskite semiconductors Cs2SnI6 and Cs2TeI6, J. Am. Chem. Soc. 138 (27) (2016) 8453–8464.

[28] A.H. Slavney, B. Connor, L. Leppert, H.I. Karunadasa, Chem. Sci. 10 (48) (2019) 11041–11053, https://doi.org/10.1039/C9SC03219C.

[29] Le-Ping Miao, Ning Ding, Na Wang, Chao Shi, Heng-Yun Ye, Linglong Li, Ye-Feng Yao, Shuai Dong, Yi Zhang, Nat. Mater. 21 (2022) 1158–1164, https://doi.org/10.1038/s41563-022-01322-1.

[30] Wei-Qiang Liao, Dewei Zhao, Yuan-Yuan Tang, Yi Zhang, Peng-Fei Li, Ping-Ping Shi, Xiao-Gang Chen, Yu-Meng You, Ren-Gen Xiong, RESEARCH, REPORT Sci. 363 (2019) 1206–1210.

[31] Heng-Yun Ye, Jia-Zhen Ge, Yuan-Yuan Tang, Peng-Fei Li, Yi Zhang, Yu-Meng You, Ren-Gen Xiong, J. Am. Chem. Soc. 138 (40) (2016) 13175–13178.

[32] Bari Maryam, A. Bokov Alexei, Zuo-Guang Ye, J. Mater. Chem. C 9 (2021) 3096–3107.

[33] G.K. Madsen, D.J. Singh, BoltzTraP. A code for calculating band-structure dependent quantities, Comput. Phys. Commun. 175 (1) (2006) 67–71.